Materials Today Bio 23 (2023) 100832

Contents lists available at ScienceDirect

Materials Today Bio

journal homepage: www.journals.elsevier.com/materials-today-bio

SEMA4D/VEGF surface enhances endothelialization by diminished-glycolysis-mediated M2-like macrophage polarization

Yuanyuan Cui [a,b,1], Xiaomei Jiang [a,1], Maozhu Yang [b], Yinglin Yuan [a], Zili Zhou [a], Xiang Gao [a], Guiqing Jia [a], Lvzhou Cao [a], Danni Li [c], Yanshuang Zhao [d], Xin Zhang [e], Gaoping Zhao [a,b,*]

[a] Department of Gastrointestinal Surgery, Sichuan Academy of Medical Sciences & Sichuan Provincial People's Hospital, School of Medicine, University of Electronic Science and Technology of China, Chengdu, 610072, China
[b] Clinical Immunology Translational Medicine Key Laboratory of Sichuan Province, Sichuan Provincial People's Hospital, University of Electronic Science and Technology of China, Chengdu, 610072, China
[c] Department of Pharmacy, Longquanyi District of Chengdu Maternity & Child Health Care Hospital, Chengdu, 610072, China
[d] Department of Pharmacy, The People's Hospital of Leshan, Leshan, China
[e] School of Mechanical and Electrical Engineering, University of Electronic Science and Technology of China, Chengdu, 610072, China

ARTICLE INFO

Keywords:
Semaphorin 4D (SEMA4D)
Vascular endothelial growth factor (VEGF)
Endothelialization
Immunometabolism
M2-like macrophage phenotype

ABSTRACT

Cardiovascular disease remains the leading cause of death and morbidity worldwide. Inflammatory responses after percutaneous coronary intervention led to neoathrosclerosis and in-stent restenosis and thus increase the risk of adverse clinical outcomes. In this work, a metabolism reshaped surface is engineered, which combines the decreased glycolysis promoting, M2-like macrophage polarization, and rapid endothelialization property. Anionic heparin plays as a linker and mediates cationic SEMA4D and VEGF to graft electronically onto PLL surfaces. The system composed by anticoagulant heparin, immunoregulatory SEMA4D and angiogenic VEGF endows the scaffold with significant inhibition of platelets, fibrinogen and anti-thrombogenic properties, also noteworthy immunometabolism reprogram, anti-inflammation M2-like polarization and finally leading to rapid endothelializaiton performances. Our research indicates that the immunometabolism method can accurately reflect the immune state of modified surfaces. It is envisioned immunometabolism study will open an avenue to the surface engineering of vascular implants for better clinical outcomes.

1. Introduction

Cardiovascular diseases (CVDs) are recognized as structural and functional disorders in heart and blood vessels. The World Health Organization estimated that more than 23.6 million people would die from CVDs by 2030 [1]. The first priority for surface modification of cardiovascular devices is inhibition of platelet adhesion and improve the hemocompatibility of these biomaterials [2]. Rapid endothelialization of cardiovascular devices could provide an efficient anticoagulant surface to prevent unwanted blood-clotting, and inhibit subsequent hemodynamic instability, bleeding complications and organ damage may follow the blood coagulation [3]. Besides hemocompatibility, restenosis is another factor which seriously impact the clinical outcome of stents and other cardiovascular devices. As a mitigation strategy, anti-proliferative drug-eluting stents (DES) have replaced bare-metal stets (BMS) and been widely applied to open blocked arteries and inhibit in-stent restenosis [4,5]. However, restenosis still be the major issue limiting the long-term efficacy of DES.

Recent studies have noticed that inflammatory plays an important role in preventing restenosis and thrombosis [6,7]. Inflammation induced endothelial dysfunction and increased lipoproteins permeability through endothelium and subendothelial lipoproteins

Abbreviations: **SEMA4D**, semaphorin 4D; **VEGF**, vascular endothelial growth factor; **CVDs**, cardiovascular diseases; **DES**, drug-eluting stents; **BMS**, bare-metal stets; **FAO**, fatty acid oxidation; **CCTA**, coronary computed angiography; **FAI**, fat attenuation index; **ETC**, electron transfer chain; **NO**, nitric oxide; **ECAR**, extracellular acidification rate; **OCR**, oxygen consumption rate; **SMCs**, smooth muscle cells; **FA**, fatty acid; **GLUT3**, glucose transporter 3; **PPP**, pentose phosphate pathway; **ROS**, reactive oxygen species; **TNF**, tumor necrosis factor; **OXPHOS**, oxidative phosphorylation; **DC**, dendritic cell.

* Corresponding author. Department of Gastrointestinal Surgery, Sichuan Academy of Medical Sciences & Sichuan Provincial People's Hospital, School of Medicine, University of Electronic Science and Technology of China, Chengdu, 610072, China.
E-mail address: gzhao@uestc.edu.cn (G. Zhao).

[1] These authors contribute equally.

https://doi.org/10.1016/j.mtbio.2023.100832
Received 27 June 2023; Received in revised form 20 September 2023; Accepted 12 October 2023
Available online 20 October 2023

accumulation, leukocyte recruitment, and platelets activation, thus contributing to neoatherosclerosis development—one of the main reasons for stent restenosis after stent implantation [8]. Histologically, apoptosis of macrophages contributes to the formation of necrotic core and calcification during neoatherosclerosis after stent implantation. Macrophages, which predominantly derived from circulating monocytes and local proliferation, increase up to 20-fold in quantity during atherogenesis, and contribute to the maintenance of the local inflammatory response by secreting pro-inflammatory cytokines, chemokines, and producing reactive oxygen and nitrogen species [9]. Environmental stimuli promote macrophages differentiate toward classical M1 macrophages, with proinflammatory properties, or alternative M2-like macrophages, which have anti-inflammatory properties. Fueled primarily by glycolysis, M1 macrophages produce high levels of proinflammatory cytokines, such as IL-6, IL-1β, TNF-α, and contribute to microbicidal activity and tissue destruction [10]. Fueled mainly by fatty acid oxidation (FAO), M2 macrophages secrete anti-inflammatory factors such as the IL-1 receptor agonist, IL-10 and collagen, and play an important role for immunity to parasites, wound healing, prevention of atherosclerosis and metabolic homeostasis [9,11]. Local inflammation status, especially macrophage phenotype and functionality, can regulate aggressive neointimal proliferation, neoatherosclerosis and in consequence in-stent restenosis [12–15].

Altered metabolism dictates macrophage's function and subsequent disease progression during atherosclerosis, in which macrophages play central roles in initiation, growth, and ultimately rupture of atherosclerotic plaques [16]. Available data about macrophage immunometabolism after cardiovascular scaffold implantation are scarce. This is due to the scarcity of macrophages, and the existing knowledge is largely based on transcriptomics and the use of genetically deficient animal model. Nowadays, coronary computed angiography (CCTA) is the most promising non-invasive method to predicate or capture coronary inflammation [17,18]. Coronary artery inflammation inhibits adipogenesis in adjacent perivascular fat, thus a novel imaging biomarker-the perivascular fat attenuation index (FAI)-can be used as a prognostic indicator to predict in-stent restenosis and severity after stent implantation [19]. The use of FAI highlights metabolism data can directly reflect the status of in-stent inflammation. From this perspective, it is necessary to study the macrophage immunometabolism of modified scaffold to analysis the precise inflammatory status around implanted grafts.

Semaphorin 4D, SEMA4D, or CD100, belongs to fourth class of semaphorin protein family, and is one of so called "immune semaphorins" [20]. SEMA4D is expressed by most of the hematopoietic cells, including lymphoid cells such as B^{21} and T [21–24] lymphocytes, natural killer cells [25], as well as myeloid cells (neutrophils [26], platelets [26] and monocytes [27–29]) and endothelial cells [30]. Our previous studies demonstrate SEMA4D modified grafts can promote rapid endothelialization and exert an immunomodulatory effect by transforming macrophages into M2-like phenotype [31,32]. Macrophages display preferential adhering and spreading onto SEMA4D rich surface, illustrating SEMA4D could promoting polarization of macrophages [33]. Vascular endothelial growth factor (VEGF) is an endothelial cell-specific mitogen in vitro and an angiogenic inducer in a variety of in vivo models [34]'. Recent research demonstrated VEGF and SEMA4D have synergistic effects on the promotion of angiogenesis in epithelial ovarian cancer [35]. In this work, SEMA4D modified surfaces [32] were optimized by introducing VEGF cytokine. We present here a novel construction of SEMA4D/VEGF modified surfaces, taking advantage of the immune regulated and endothelialization promoted property of SEMA4D and the pro-angiogenic characteristic of VEGF. Furthermore, immunometabolism methods were innovatively used to evaluate the functioning of macrophages contacting modified surfaces.

2. Materials and methods

2.1. Materials

Biomedial titanium samples (99.9 % Ti, 10 mm diameter) were used. Namely, thin titanium plates firstly were mirror polished, then cleaned three times separately by acetone, alcohol and finally by reverse osmosis (RO) water. SEMA4D and VEGF were purchased from PeproTech Inc. (Rocky Hill, United States). Low molecular heparin (MW < 8,000, potency >160U/mg) was purchased from Shanghai Bioscience & Technology company (Shanghai, People's Republic of China). Dopamine, Polylysine (PLL, 150,000–300,000), DAPI (4′,6-diamidino-2-phenylindole), rhodamin were purchased form Sigma-Aldrich (Saint Louis, MO). The related materials used in Glycolytic Rate Assay were all purchase from Seahorse Bioscience (California, United States).

2.2. SEMA4D and VEGF modification

The detailed modification steps are exhibited in Fig. 1 A. Namely, polished Ti were immersed in 2 M sodium hydroxide solution at 80 °C for 12h to activate Ti plates, denoted as Ti–OH. After washing PLL (2.5 mg/mL) were modified by incubating at 4°C overnight to get rich amino Ti-PLL. SEMA4D/heparin complexes were prepared by blending equal volume of SEMA4D (200 ng/mL) and heparin (10 mg/mL), then were added onto PLL-Ti plated for at least 3h at 37 °C , and named as V0. Further, 200 ng/mL VEGF was added onto V0 37 °C for 3h, then thoroughly washed with three times of PBS, thus these VEGF incubation samples were specified as V200.

2.3. X-ray photo electron spectroscopy (XPS)

The modified surface elemental composition was analyzed by XPS on an AXIS His spectrometer (Kratos Ltd., Manchester, United Kingdom) with a monochromatic Al Ka X-ray source (1486.6 eV photons, 150W) and chamber pressure below 2×10^{-9} Torr. Binding energy was referenced by setting the C1s peak at 284.6 eV.

2.4. Platelets adhesion and activation

Anticoagulated healthy human whole blood ($V_{3.8\ \%\ citrate}$:V_{blood} = 1:9) donated by healthy volunteers was centrifuged at 1500r/min for 15min. Experiments were carried out within 12h after the blood collection.

Platelet-rich plasma (PRP) was obtained by low centrifugation of fresh human blood (1500 rpm, 15min), then 50 μl PRP was added on modified samples and incubated for 1h. After gently washed with PBS, 2.5 % glutaraldehyde was used to fix platelets adhering on modified samples. After overnight fixation, dehydration and dealcoholization, PRP incubated samples were photographed using a flurescence microscopy to evaluate platelet number. The average density of platelet number on each sample was determined by 18 random images. Field-emission scanning electron microscopy (SEM, jsm-7001F, JEOL Ltd., Japan) was used to evaluate the morphology of platelets adhering on modified samples.

Activated platelets were quantified by determining the expression of P-selection, a activated platelet marker. Briefly, 20 μl PRP was added onto the modified samples and incubated at 37 °C for 1h, then washed with PBS for three times. After blocking by 1 % bovine serum albumin (BSA), mouse antihuman P-selectin antibody (1:800 in pH7.4 PBS) used as first antibody was added and incubated at 37 °C for 1h. Horse-radish peroxidase (HRP)-labeled goat antimouse IgG as the second antibody was added and incubated for another 1h at 37 °C. Then TMB as chromogenic agent was added and incubated for 10 min. Finally, 1 M H_2SO_4 was used to stop above color reaction. A 150 μl of reaction solution was transferred to a new 96-well plate and measured at 450 nm.

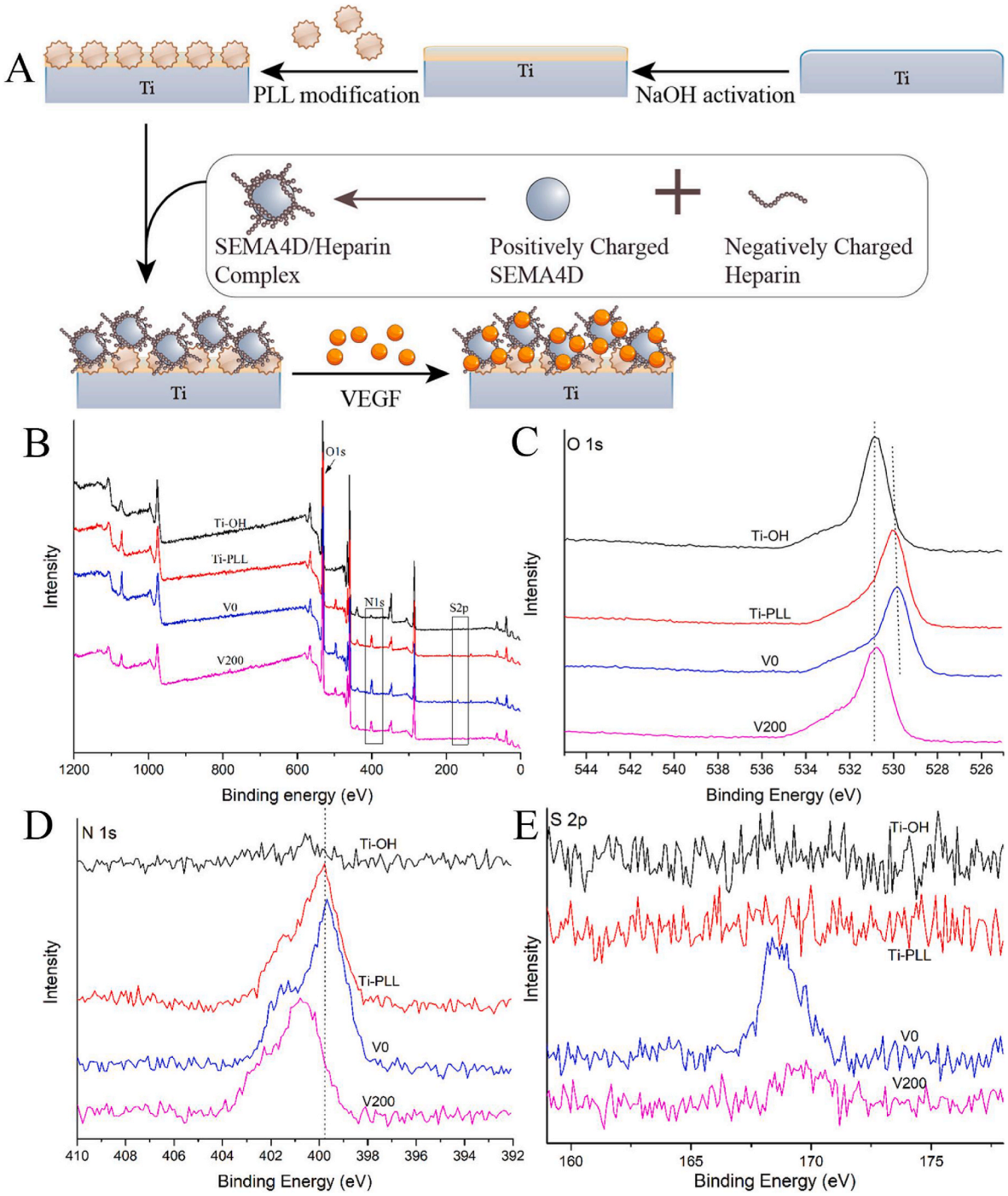

F

Sample ID	C (%)	N(%)	O(%)	S(%)
Ti-OH	49.63	0	50.37	0
Ti-PLL	47.52	7.05	45.43	0
V0	48.95	7.67	42.02	1.37
V200	48.65	5.65	44.94	0.75

Fig. 1. Schematic diagram and XPS results. (A) Schematic diagram of V0 and V200 modified samples; (B) Representative XPS survey spectra of 4 samples (Ti–OH, Ti-PLL, V0 and V200); (C) XPS high-resolution spectra of O1s peaks; (D) XPS high-resolution spectra of N1s peaks; (E) XPS high-resolution spectra of S2p peaks; (F) Elemental composition (C, N, O, S) of 4 samples.

2.5. Fibrinogen binding and conformation change

Fibrinogen binding is a central process inducing thrombus formation, directly determining the blood compatibility of bio-materials. In detail, fresh human blood was centrifuged at3,000 rpm for 15 min, and thus to obtain pletelet poor plasma (PPP). For fibrinogen binding assay, 50 μl PPP was added onto modified samples and incubated for 1h at 37 °C. After block reaction by 1 % BSA and washed by three times of PBS, samples were immersed in 30 μl first antibody (HRP-conjugated mouse antihuman fibrnogen antibody, 1:10,000) and incubated for 1h at 37 °C. After wash of three times of PBS, 80 μl TMB was added and incubated for 10 min for color reaction. Following stop reaction by 1 M H_2SO_4, 150 μl of above reaction solution was transferred to a 96 well plate and measured at 450 nm to assay the density of binding fibrinogen.

Fibrinogen conformation change assay mainly evaluates the exposure of fibrinogen γ-chain. In detail, 50 μl PPP was added onto modified samples and incubated for 1h at 37 °C. After block reaction by 1 % BSA and washed by three times of PBS, samples were immersed in 30 μl first antibody (HRP-conjugated mouse monoclonal anti-human fibrinogen γ-chain antibody, 1:5000) and incubated for 1h at 37 °C. The following steps was the same as above fibrinogen binding assay.

2.6. Cell isolation and culture

Human umbilical vein endothelial cells (HUVECs) were isolated and cultured as previous works [31,32]. Briefly, after wash by PBS and check the integrity of umbilical cord, DEMEM/F-12 containing 0.1 % type 2 collagenase was injected into umbilical vein and incubated for 15 min at 37 °C with occasionally kneading. Subsequently, DEMEM/F-12 containing 5 % fetal bovine serum (FBS) was injected into umbilical vein to inhibit digest reaction. Collect all solution in the umbilical vein and centrifugate at 1200 rpm for 8 min, harvested cells are the goal cells, HUVECs. Cells were re-suspended with DMED/F-12 basic medium containing 15%FBS, 1 % L-glutamin, and 20 μl/ml endothelial cell growth supplement and cultured under humidified incubator with 5% CO_2 at 37 °C.

2.7. Cell proliferation assay

HUVECs were cultured on modified samples with a density of 5×10^4 cells/ml under 5%CO_2 at 37 °C. At each scheduled time point, after gently wash by PBS, 400 μl culture medium (DMED/F-12 basic medium with10%FBS) containing 10 % CCK-8 reagent was added to each sample well and incubated for 3h. 200 μl CCK-8 containing medium was collected and transferred to 96-well plate and measured at 450 nm. Each sample assay was performed in triplicate.

2.8. Fluorescence staining

Briefly, after cell incubation and gently wash by PBS, 2.5 % glutaraldehyde was added to each sample well to fix cells on samples. 20 μg/ml Rhodamin 123 was added and incubated for 15 min to dye cell. After wash by PBS, the morphology and density of cells on modified samples could be observed and photographed under Leica DMRX fluorescence microscope (DMRX, lEICA, Germany).

2.9. Chemotaxis and hypotaxis assay

Chemotaxis assay was carried out by using 0.45 μm Boyden chamber. Briefly, HUVECs was collected and seeded in Boyden chamber at a density of 3×10^5 cell/ml and incubated for 12h. 100 μl suspended cell medium was added into up chamber, 600 μl culture medium without cells and modified samples were added into low chamber. At pointed time, after gently wash, Boyden chambers were immersed in fixation solution (methanol) for 12h. Removing the cells on inner part of chamber film, then dying cells on outer part of chamber film by DAPI for 30 min, ECs transferred through Boyden chamber could be evaluated by using Leica DMRX fluorescence microscope.

Hypotaxis assay was performed as following. Briefly, samples (size: 2×1 cm) were vertically half folded, one half was unmodified Ti surface, and the other half was modified surface. HUVECs (5×10^5 cell/cm^2) were seeded onto unmodified Ti surface and incubated until to form a confluent monolayer. Transfer samples to a new plate and vertically turn over to observe cells migrate distance on modified samples.

2.10. Implantation assay

Nine-week-old SD male rats were used to assay in vivo endothelialization of modified samples. Briefly, rat abdominal aorta was separated and blocked by hemostatic clamps. Modified samples (3 cm wire) were implanted into aorta through minimally invasive method [32]. At the 21st day, implanted samples together with arterial blood vessels were harvested. After fixation of 4 % paraformaldehyde solution for 24h, aorta were paraffin embedded and subsequently subjected to HE (hematoxylin and eosin) and immunofluorescence (rabbit anti-rat CD31 and rabbit anti-rat α-SMA) staining. DAPI was used for staining cell nuclei.

2.11. Glycolytic Rate Assay

Glycolytic rate assay evaluates the rate cells converting glucose to lactate, carried out according to Agilent Seahorse XFp Glycolytic Rate Assay Kit. Briefly, at the day prior to assay, open Agilent Seahorse XFp machine to reheat system. Hydrate the sensor cartridge in agilent seahorse XF calibrant at 37 °C in a non-CO2 incubator overnight. 100 μl poly-D-Lysine (100 μg/ml in PBS) was added to each well of the seahorse cell micro-plates and incubated for 30 min, washed by UP water and stored at room temperature. At the day of assay, 50 μl of THP-1(40K total amount) was added into each well, centrifuge (200G) gently to promote cell adhere. Then gently add another 130 μl assay medium to each well and incubate the seahorse micro-plate at 37 °C in a non-CO_2 incubator for 50 min. Add 20 μl corresponding compounds (assay medium for control, 100 ng/ml SEMA4D for V0, and 100 ng/ml SEMA4D + 200 ng/ml VEGF for V200) to port A of sensor cartridge. Load 22 μl Rot/AA (rotenone, 5 μM) to port B and 22 μl 2-DG (2 deoxyglucose, 500 mM) to port C. Running assay according to the directions of seahorse machine. Every experiment has been repeated for three times and considered trustworthy when the results of these three times have the same trend. There were two parallel samples for each sample because Agilent Seahorse XFp only have 6 operation wells.

2.12. Immune factors detection

THP-1 cells co-cultured with modified samples for 3 days, then supernatant was collected and preserved at −20 °C. Immune factor evaluation (IL-10, IL-6 and TNF-α) was carried out according to kit manual (human IL-10, IL-6 and TNF-α , NEOBIOSCENCE). First, 100 μl supernatant was added to the corresponding 96 well and cultured at 37 °C for 90min under light proof condition. After 5 times washing, 100 μl enzyme binding substrate was further added and cultured at 37 °C for 30min under light proof condition. Following 5 times of wash, 100 μl chromogenic substrate (TMB) was added and cultured at 37 °C for 15min under dark condition. 100 μl reaction termination solution was added to stop chromogenic reaction and directly measured at 450 nm.

2.13. Flow cytometry

THP-1 co-cultured with modified samples for 3 days, were collected and stained for the following flow cytometry. For the detection of intracellular molecules, cells were fixed and permeabilised with the BD Cytofix/Cytoperm kit according to the manufacturer's instructions. The

BD antibodies were used for flow cytometry: Fluorescein isothiocyanate (FITC)-conjugated CD86; phycoerythrin (PE)-conjugated CD68; phycoerythrinc-yanine 7 (PE-Cy7)-conjugated CD206; peridinin-chlorophyll cyanine 5.5 (PerCP-Cy5.5)-conjugated CD14.

2.14. Western blotting

THP-1 were cultured with different modified samples for three days and then collected and homogenized in ice-cold RIPA lysis buffer. The protein contents were determined by the bicinchoninic acid (BCA) kit (Solarbio PC0020, China), and the cellular lysates were separated by 8 % SDS-PAGE and transferred onto polyvinylidene fluoride (PVDF) membranes. After being blocked with 10 % non-fat milk in TBST, the membranes were incubated with primary antibodies (Anti-Glucose Transporter GLUT3 Recombinant Rabbit Monoclonal Antibody, ET1704-59; Anti-PGK1 Recombinant Rabbit Monoclonal Antibody, ET1609-63, Huabio, China) at 4 °C overnight, followed by 1:000 horseradish peroxidase (HRP)-conjugated secondary antibody (Anti-rabbit IgG, HRP-linked Antibody,7074, CST, USA) for 1hr. Immunoreactive bands were visualized using an enhanced chemiluminescence kit (EBLOT, China).

3. Results

3.1. Successful modification of SEMA4D and VEGF detect by XPS

Element composition of the SEMA4D and VEGF modified surfaces was detected by using XPS (Fig. 1 B, C, D, E and F). Element O (Fig. 1 B, C and F) mainly derived from hydroxyl group of Ti–OH, reaches to 50 % after alkali activation. PLL, containing large amount of amino group ($-NH_2$), would consume part of hydroxyl group, decrease element O to 45.43 %, meaning the successful fixation of PLL. SEMA4D/Heparin complex has excessive heparin would further consume surface hydroxyl group, and decrease element O to 42.02 %, illustrating the successful modification of SEMA4D/Heparin complex. VEGF, containing an isoelectric point of 8.5, would dissociate some hydroxyl group when environmental pH (pH7.4) is lower than 8.5. Thus, VEGF modification can raise element O in some degree (from 42.02 % to 44.94 %).

PLL contains large amount of amino group ($-NH_2$) and contributes to the most content of element N (Fig. 1 B, D and F). After PLL modification on Ti–OH samples, the concentration of element N increased largely from 0 to 7.05 %. The rest small part of element N derived from heparin, a kind of mucopolysaccharide sulfate molecule containing little content of sulfamic group ($–NHSO_3–$). When after SEMA4D/Heparin complex modified on PLL samples, there was a small degree of raise in element N, illustrating the SEMA4D/Heparin complex have been successfully fixed

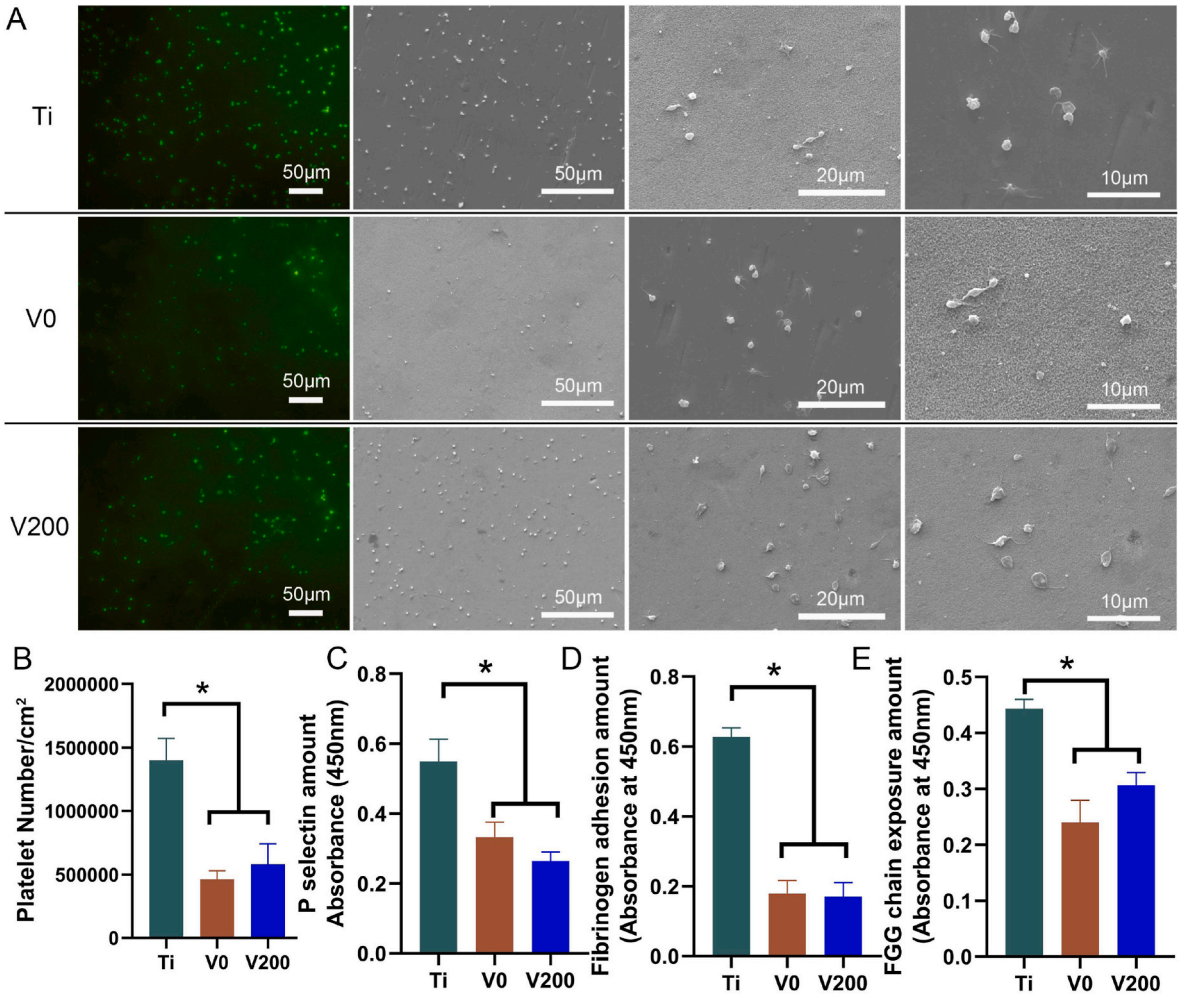

Fig. 2. Hemocompatibility results. (A) Immunofluorescence images (green) and SEM images of adhering platelets; (B) Platelet number adhering on modified samples after incubating with PRP; (C) P selectin denotes the activation degree of adhering platelet; (E) Fibrinogen adhesion amount on modified samples after incubating with PPP; (E) FGG exposure amount for modified surfaces. Data presented as mean ± SD (n = 4) and analyzed using a one-way ANOVA, *P < 0.05 compare Ti with other samples. (For interpretation of the references to colour in this figure legend, the reader is referred to the Web version of this article.)

onto PLL samples. VEGF, containing an isoelectric point of 8.5, can bind to sulfamic group (–$NHSO_3$–) and other anionic group from heparin via electrostatic force. The modification of VEGF would cover the surface sulfamic group (–$NHSO_3$–) of heparin, and decrease the content of element N from 7.67 % to 5.65 %, indicating the successful modification of VEGF.

Heparin completely contributes to the element S (Fig. 1 B, E and F). The successful modification of SEMA4D/heparin complex increase the element S from 0 to 1.37 %. Subsequently binding of VEGF shelters the heparin, and decrease element S from 1.37 % to 0.75 %, delineating the successfully modification of VEGF.

3.2. Blood compatibility after modification of SEMA4D and VEGF

3.2.1. Platelets adhesion and activation

The adhesion and activation degree of platelet and fibrinogen directly determine the healing of vulnus. After 1h incubation of PRP on different samples, the immunofluorenscenc showed the adhere platelets on modified samples V0 and V200 were much lesser than non-modified sample Ti (Fig. 2 A and B). Modified samples V0 and V200 containing large amount of heparin (Fig. 1 F), which can effectively reduce the adhesion of platelets. Notably, VEGF modification (V0) consumes part of heparin compared to V0, resulting a little higher level of adhere platelets. The trend of adhesion platelet on samples (Fig. 2 B) was similar to the trend of FGG chain amount (Fig. 2 E), indicating fibrinogen may mediated the adhesion and aggregation of platelet [38]. SEM pictures (Fig. 2 A SEM) indicates that compared to non-modified Ti samples, the platelets adhering on V0 and V200 aggregate less, and have fewer dendritic or pseudopodia-like protrusions, indicating the platelets on modified samples are less activated. This data was further verified by the amount of selectin P (Fig. 2C), a marker of activated platelets. V0 has a higher level of platelet activation compered to V200 due to the pro-activating effect of SEMA4D on the platelet [26].

3.2.2. Fibrinogen adhesion and conformational change

Fibrinogen adhesion and conformation change (fibrinogen activation, namely FGG chain exposure) can induce platelet aggregation and activation. The activation of plasma coagulation system in mammalian blood causes the polymerization of fibrin and the activation of platelets, ultimately leading to a blood clot [36]. As an indirect anticoagulant, heparin can achieve anti-coagulation by activating antithrombin (AT), which can inhibit thrombin activity [37], or by directly inhibiting coagulation factors in other coagulation pathways such as factors IXa, Xa, and XIa. After 1h incubation of PPP with samples, it is showed fibrinogen adhesion amount and FGG chain exposure amount on modified samples V0 and V200 are much lesser than non-modified sample Ti (Fig. 2 D and E), indicating heparin modified on samples V0 and V200 play a key role in inhibiting fibrinogen adhesion and subsequent FGG chain exposure. VEGF shelters part of surface heparin on V200, resulting a little bit higher activation of fibrinogen (Fig. 2E).

3.3. Endothelial cell proliferation and migration on SEMA4D and VEGF modified samples

Rapid endothelialization can promote healing. HUVECs were seeded on samples for 1 and 3 days (Fig. 3 C). Without molecules modification, the cells cultured on Ti had a proliferation rate of 0.9. SEMA4D/Heparin complex modified sample V0 had a proliferation rate of 0.92, slightly

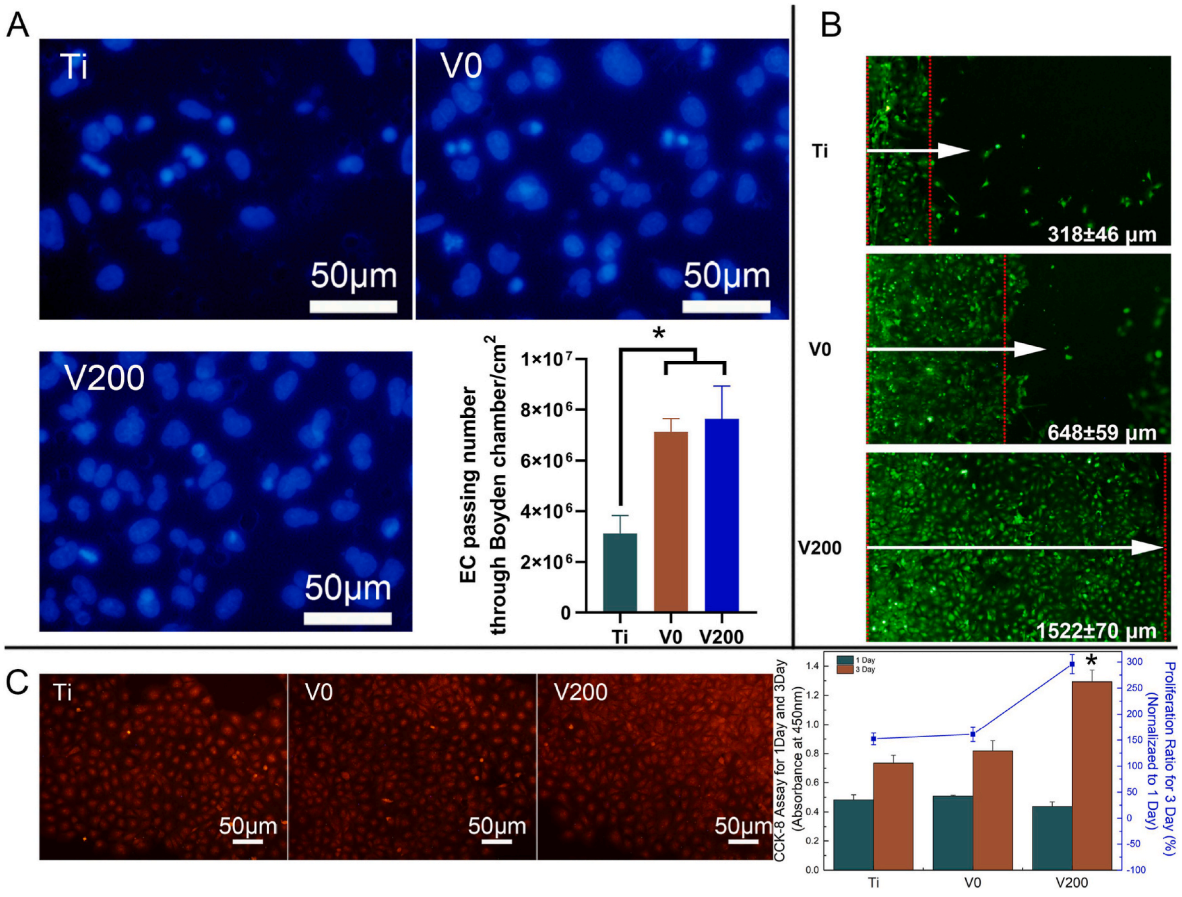

Fig. 3. EC proliferation and migration. (A) EC chemotaxis assay using the Boyden chamber and corresponding immunofluorescence image of the nucleus; (B) EC haptotaxis assay on modified samples; (C) EC proliferation results after 1- and 3-day culture on modified samples. Data presented as mean ± SD (n = 5) and analyzed using a one-way ANOVA, $^*P < 0.05$ compare Ti with other samples.

higher than cells on Ti. Further modified by VEGF, sample V200 had a relatively high EC proliferation rate of 1.4, indicating VEGF plays an important role of promoting EC proliferation.

Chemotaxis migration means cells moving with directional preference according to soluble molecules. While haptotaxis migration refers to the movement of cells in response to chemical stimulus from adherent molecules. Chemotaxis migration was carried out by using Boyden chamber assay (Fig. 3 A). Compared to non-modified Ti samples, HUVECs cultured with V0 and V200 in Boyden chambers showed a significant chemotaxis migration. SEMA4D and VEGF both can acts as potential chemoattractant [39,40], thus promoting the EC chemotaxis migration in Boyden chamber containing V200 and V0 modified samples. Meanwhile, haptotaxis migration of ECs is an important process of promoting endothelium regeneration as wound healing. Haptotaxis migration assay on different samples showed modified samples V200 and V0 can promote EC adhering, spreading, proliferation and regeneration. ECs on SEMA4D modified samples V0 had a twice haptotaxis migration distance of that on Ti control sample (648 μm vs 318 μm).

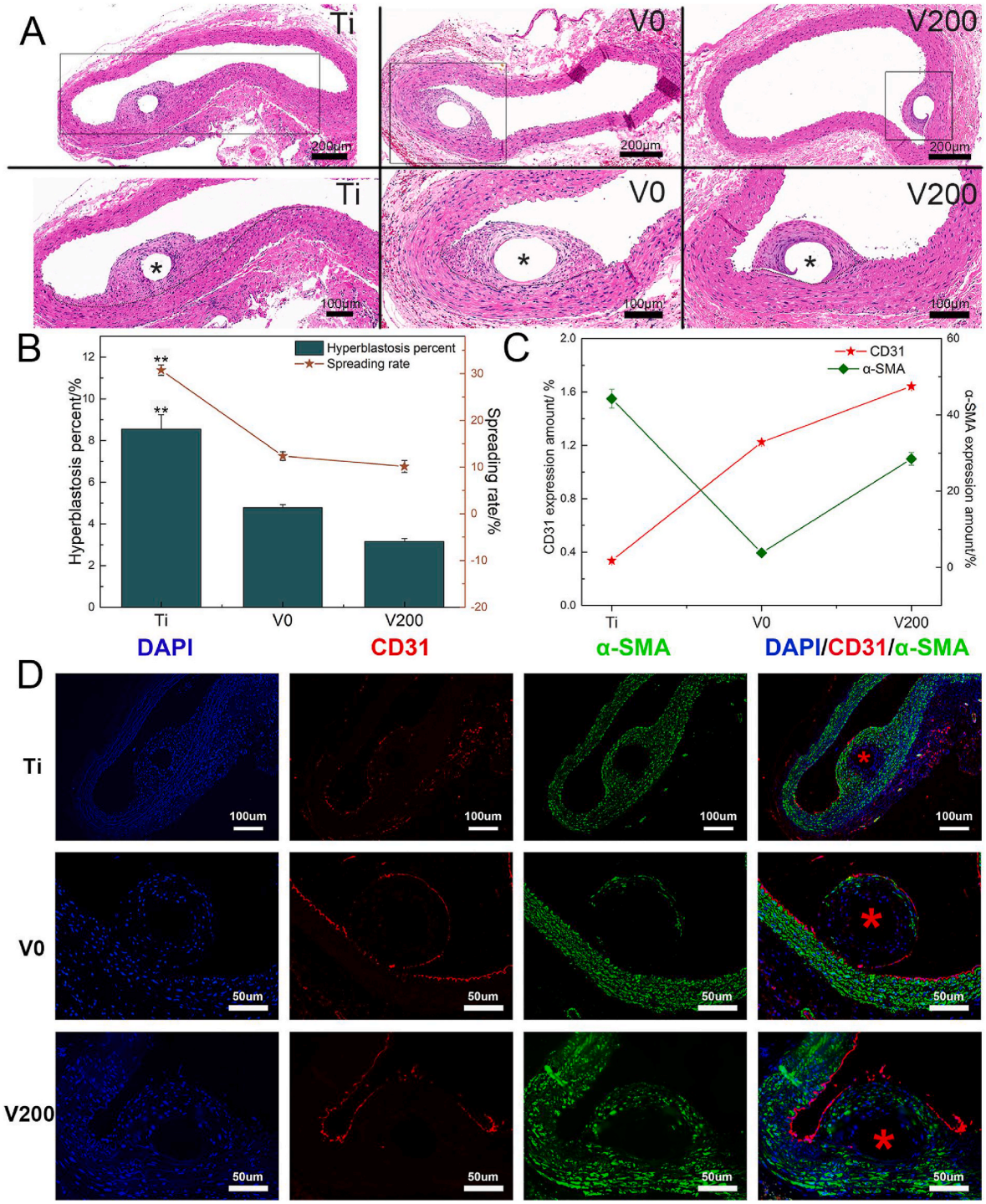

Fig. 4. In vivo transplantation. (A) HE staining images shows the morphologies of neo-tissues; (B) Hyperblastosis percent and spreading rate of the neo-tissues; Neo-tissue immunofluorenscent staining by CD31 and α-SMA (D) and corresponding expression amount (C). Data presented as mean ± SD (n = 4) and analyzed using a one-way ANOVA, $^{**}P < 0.05$ compare Ti with other samples (* indicates the implanted sites of samples).

SEMA4D directly active intracellular tyrosine kinase cascades of PI3K-Akt pathway via its high affinity receptor plexinB1, thus promoting cell adhesion, cell proliferation and exerting a pro-angiogenic effect [41]. ECs on SEMA4D and VEGF dual modified samples V200 migrated a four time more distance than the distance ECs migrating on Ti. It was recently reported VEGF and SEMA4D have synergistic effects on the promotion of angiogenesis [35].

3.4. In vivo assay

Vessel injury and inflammation cause vascular smooth muscle cells (SMCs) dedifferentiation, migration, proliferation and secretion of extra-cellular matrix into the vessel's innermost layer or intima, finally the presence of intimal hyperplasia [42]. Anti-inflammation or low level of inflammation would alleviate intimal hyperplasia. Here we use hyperblastosis percent implies the degree of intimal hyperplasia, and spreading rate means the degree neo-tissue occupying original endodermis. After in vivo implantation of samples in rat aortaventralis for 21 days, in situ endothelialization happened on the wire samples in different extent (Fig. 4). HE showed neo-tissues around V200 samples had smallest degree of intimal hyperplasia (2.6 %) and spreading rate (10 %) (Fig. 4 A and B), delineating a best healing of V200. SEMA4D modified sample V0 showed a second smallest intimal hyperplasia (4.4 %) and spreading rate (13 %), suggesting the endothelialization is weakened without VEGF involvement. A large neo-tissue was formed around Ti samples, representing the biggest intimal hyperplasia of 8.4 % and spreading rate of 30.7 %, suggesting an inflammation environment around Ti samples and a largest disturbance of neo-tissues around Ti samples to the original endodermis.

Immunofluorescent staining was further carried out to determine the percentage of endothelial cell (marked by CD31) and SMCs (marked by α-SMA) in neo-tissues formed around different samples (Fig. 4C and D). The neo-tissues around Ti had the highest percentage of SMCs (47 %) and lowest percentage of endothelial cells (0.35 %), suggesting a worst endothelialization and worst inflammation environment on Ti samples. Compared to V0, neo-tissues formed around V200 had a higher percentage of endodermis (1.65 % vs 1.2 %) and SMCs (28 % vs 3 % 20 %) , indicating a better endothelialization of V200 than V0, and lower inflammation environment around V200.

3.5. Inflammation effect and macrophage phenotype polarization

Inflammation and proliferation of vascular SMCs are the key events in intimal hyperplasia around modified samples. Inflammatory factors and cell phenotype directly determined the processes of endothelialization and intimal hyperplasia of neo-tissues, and detected after macrophage THP-1 co-cultured with modified samples for 3 days (Fig. 5). IL-10, an anti-inflammation factor, secreted by THP-1 cultured with V200 and V0 was higher than bank control and Ti, illustrating that the inflammation of THP-1cultured on V200 and V0 is lower. Compared to V200, VEGF modified V0 promoted a higher amount of secreted IL-10 (Fig. 5 A). The pro-inflammatory factors, IL-6 and TNF-α, were also the lowest after THP-1 co-cultured with V0, further indicating V0 modified samples possess the lowest inflammatory characteristics (Fig. 5 B and C).

Macrophages are heterogeneous and plastic cells, able to be polarized into pro-inflammatory M1 phenotype and anti-inflammatory M2-like phenotype dynamically [43]. After co-cultured with samples for 3 days, the phenotype of THP-1 changed according to different stimulus of co-cultured samples. THP-1 first differentiated into M0 phenotype (CD14 as the marker), and then M0 phenotype polarized into M1 (CD206 as the marker) or M2 (CD86 as the marker) phenotype (Fig. 5 D, E, F and G). The flow cytometry results showed V200 stimulates the highest amount of M0 (7.91 %), Ti and V0 stimulate the similar amount of M0 (2.38 % and 2.40 % respectively). Ti sample stimulated the highest amount of pro-inflammation M1(1.24 %), modified samples V0 and V200 stimulated fewer M1, 1.11 % and 1.03 % respectively, illustrating V200 samples has the lowest pro-inflammation property. Though V0 stimulated the highest amount of M2-like phenotype in all the M0 (Fig. 5 G), considering its significant higher mount of M0 (Fig. 5 E), V200 actually stimulated the highest M2-like among M0 subset. The flow cytometry results indicated that the V200 has the lowest inflammation property, further verified the results of cytokine (Fig. 5 A, B and C).

3.6. Timely glycolysis rate and stimulated glycolysis rate

The emerging field of immunometabolism has particular relevance to the study of inflammation. Intracellular metabolic pathways also directly control the specialized effector functions of macrophage. Metabolic reprogramming between glycolysis and mitochondrial respiration is implicated in macrophage polarization. M1 macrophages primarily rely on glycolysis , block TCA cycle (tricarboxylic acid cycle), produce inflammatory intermediates (such as ROS and NO), and exert antimicrobial responses (Fig. 8). Whereas M2-like macrophages rely on TCA cycle and oxidative phosphorylation, produce anti-inflammatory cytokines and remodel tissues, such as promoting angiogenesis and remodeling extracellular matrix [44]. Thus, factors that affect macrophage metabolism may reshape M1/M2 homeostasis and change the environment inflammation, finally exert antimicrobial responses or remodel around tissues.

Our previous study demonstrated that elevated concentration of SEMA4D promotes a more rapid polarization of macrophages and a lower secretion of pro-inflammatory factor, TNF-α and IL-6 [32,33], indicating SEMA4D, not heparin, serves as a immunomodulatory factor to regulate macrophage functionality and response. Thus, we imitated the modified samples V0 and V200 by adding SEMA4D and SEMA4D/VEGF separately in glycolysis rate tests. The results of timely and stimulated glycolysis rate tests showed a same tendency with results of inflammatory factor and macrophage phenotype, further suggesting heparin plays a minimal role in immune regulation.

Glycolysis tests (Figs. 6 and 7) were carried out to detect whether glycolysis can reflect the inflammation state after corresponding stimulus. Timely glycolysis tests performed directly after stimulated cytokines added to the Seahorse reaction chamber (Fig. 6). The ECAR curve showed at beginning the metabolism rates of glucose among different samples were at the same level (the curve before timely glycolysis) (Fig. 6 A). After adding stimulus, timely glycolysis changed, both V0 and V200 induced a decreased glycolysis trend with a lowest glycolysis emerging in V200 stimuli (Fig. 6 A and C). The compounds rotenone/antimycin A (Rot/AA) specifically inhibit the electron transfer chain (ETC), maintain the metabolites of upstream glycosis, lactate, reserving in cytoplasm and not been metabolized. ECAR curve indirectly reflects the glycosis by detecting the amount of lactate. After Rot/AA inhibition, the compensatory glycolysis increased sharply (Fig. 6 A and D). Compensatory glycolysis of V0 was a little higher than control groups, probably the stimuli from V0 also cause the decreased consumption of lactate from other metabolic pathway, such as amino acid metabolism, fatty acid metabolism or other pathways lactate participated in, resulting a higher amount of lactate been preserved and thus a highest glycolytic reserve (Fig. 6 A and E). The non-glycolysis data of V0 is the highest, further suggesting lactate under V0 stimuli may participate more in other metabolic pathways but not glycolysis pathway (Fig. 6 A and F). Due to the decreased timely glycosis, the production of lactate stimulated by V200 reduced, resulting in a reduced compensatory glycolysis, and accompanying by the lowest compensatory glycolysis rate (Fig. 6 A and E). The lowest non-glycolysis of V200 manifested lactate under V200 stimuli may participate more in glycolysis pathway, not other metabolic pathways (Fig. 6 A and F). OCR curve reflects the consumption of oxygen. Most part of oxygen was consumed by the ETC pathway, and a small part of oxygen was consumed by other metabolic pathway. OCR curve showed V0 has the highest level of oxygen consumption before and after ETC inhibition, suggesting V0 stimuli may

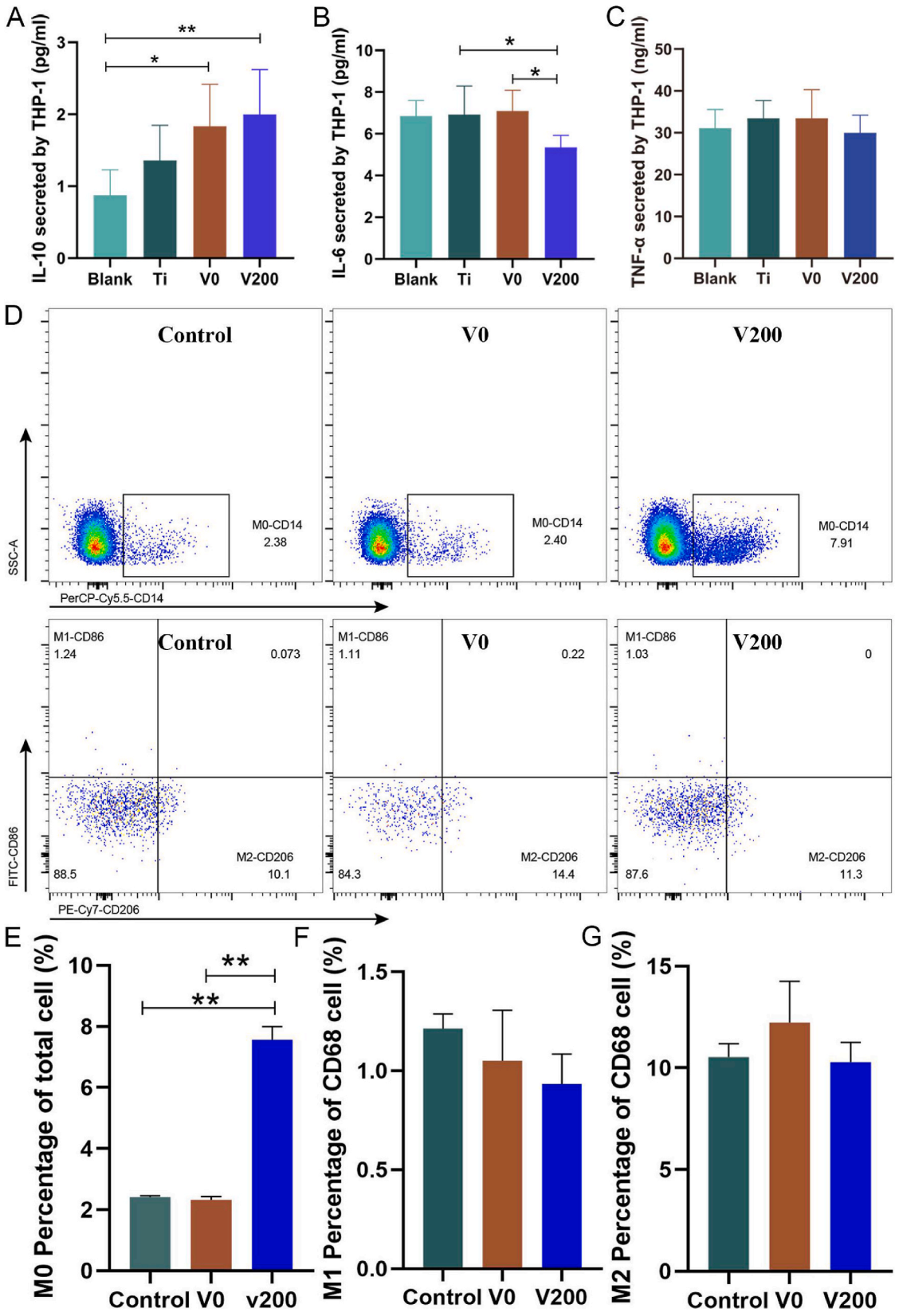

Fig. 5. Inflammatory factor and macrophage phenotype. IL-10 (A), IL-6 (B), and TNF-α (C) secreted by THP-1 after co-culturing with modified samples for 5days; (D) M0(PerP-Cy5.5-CD14), M1 (FITC-CD86) and M2 (PE-Cy7-CD206) phenotype detected by flow cytometry and their corresponding percentage after THP-1 co-cultured with SEMA4D (100 ng/ml) and SEMA4D (100 ng/ml) + VEGF (200 ng/ml) for 3 days. Data presented as mean ± SD (n = 4) and analyzed using a one-way ANOVA, $^{**}P < 0.05$.

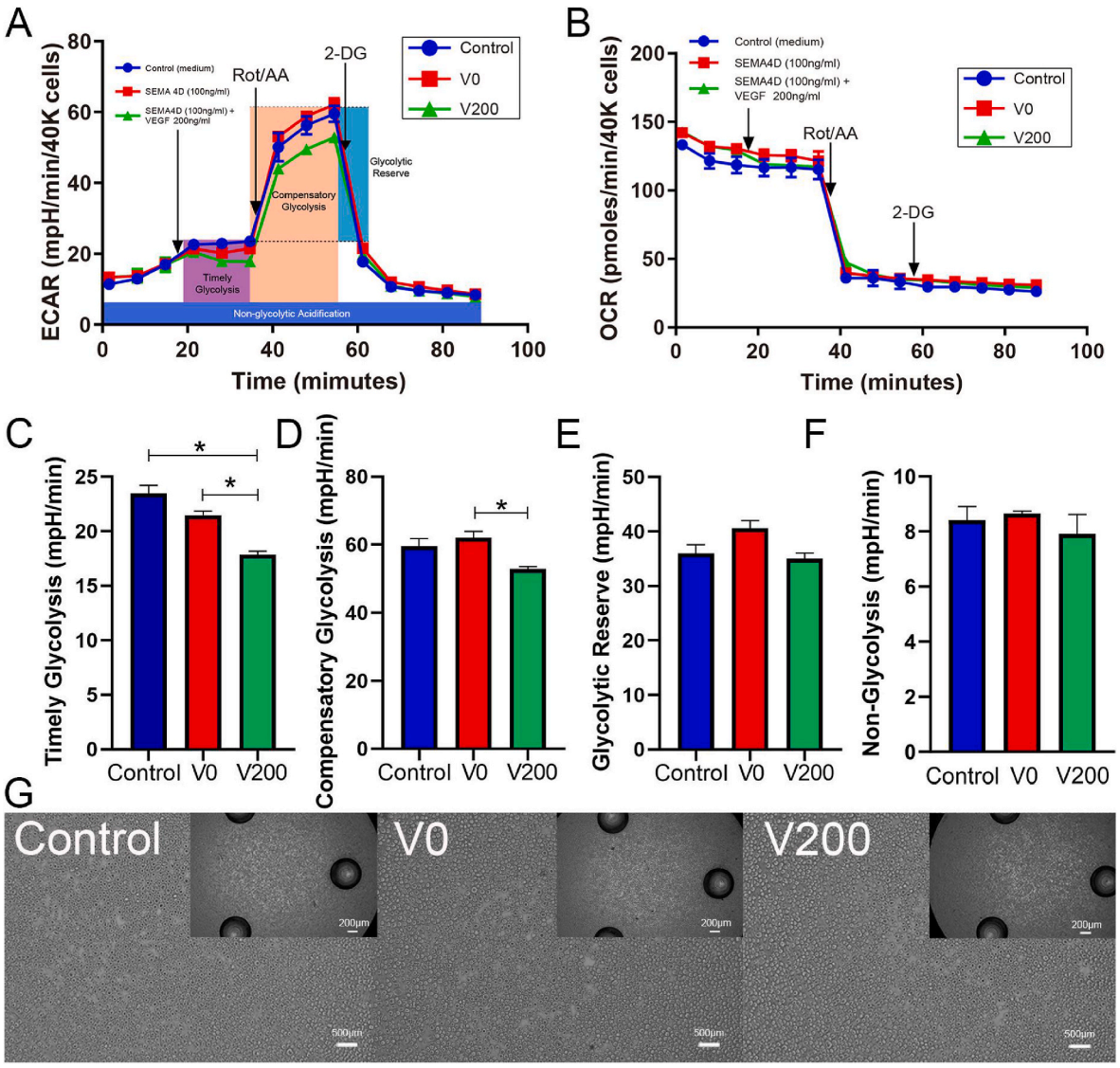

Fig. 6. Timely glycolysis rate. (A) Timely ECAR (Extracellular Acidification Rate) curve after different stimulus; (B) Corresponding OCR (Oxygen Consumption Rate) curve after different stimulus; Timely glycolysis data (C), Compensatory glycolysis data (D), Glycolytic revserve data (E) and Non-Glycolysisi data (F) of different stimulus; (G) THP-1 adhere on Seahorse chamber niformly and firmly. Data presented as mean ± SD (n = 2) and analyzed using a one-way ANOVA, $*P < 0.05$.

promote metabolic pathways beyond glycolysis to consume oxygen (Fig. 6 B). Figure G showed THP-1 adheres Seahorse chamber uniformly and firmly, this can ensure Seahorse machine capture accurate data. The timely glycolysis indicated that V0 and V200 stimulus can reduce macrophage glycolysis timely, accompanying with a largest decrease of glycolysis after V200 stimuli.

Timely ECAR showed modified samples V0 and V200 can reduce the glycolysis activity of macrophage THP-1 (Fig. 6). Considering the fact that both SEMA4D and VEGF have the isoelectric point of pH 8.5, the decrease of lactate (PI = 3.86–3.88) could be achieved via acid-base reaction between lactate and SEMA4D or VEGF. Thus, after stimulation for 3h, the new reaction solution replaced the stimulated liquid to investigate whether glycolysis of THP-1 still reduced after V0 or V200 stimulus (Fig. 7). At the beginning stage of basic glycolysis, the glycolysis levels of V0 and V200 were lower than controls (Fig. 7 A and C). The saturate glycolysis OCR had the same trend with basic and timely glycolysis level, further suggesting the decreasing oxygen demand and glycolysis activity of THP-1 cells stimulated by V0 or V200 (Fig. 7 A, C, D and I). Subsequent addition of 20 mM supersaturated glucose raised the glycolysis degree of all samples, but the timely glycolysis levels of V0 and V200 were still lower than their control peers (Fig. 7 A and D). Decreased glycolysis suggested the reduced oxygen consumption, this can be confirmed by the saturate glycolysis (Fig. 7 B and I). V200 had the lowest level of glycolysis at both basic and timely glycolysis, but highest compensatory glycolysis and highest glycolytic reserve (Fig. 7 A, E and F), suggesting the THP-1 after V200 stimuli promoted the ability of glucose reserve and the conversion efficiency of glucose to lactate. Though THP-1 after V200 stimuli had an enhanced glycolysis function, they performance a low glycolysis demand (Fig. 7 A, C, E and F). V0 and V200 stimulus had the similar non-glycolysis trend, which is lower than control peers, delineating the activities of other metabolic pathways (such as PPP, FA synthesis and glutaminolysis, pyruvate involved in other metabolic pathways can convert into lactate) were down regulated (Fig. 7 A and G). Actually, metabolism is a dynamic equilibrium process with rewiring all the other metabolic pathway (such as fatty acid synthesis, pentose phosphate pathway, glutaminolysis and oxidative phosphorylation pathway) beyond just down-regulating glocolysis when polarizing toward M2-like macrophages. Non-glycolysis and non-mitochondrial OCR showed THP-1 after V0 and V200 stimuli are down regulated their demand for oxygen in mitochondrial and glycolysis pathways, and V200 stimuli minimized the metabolic activities in glycolysis and in mitochodral when glucose inputs were inhibited (Fig. 7

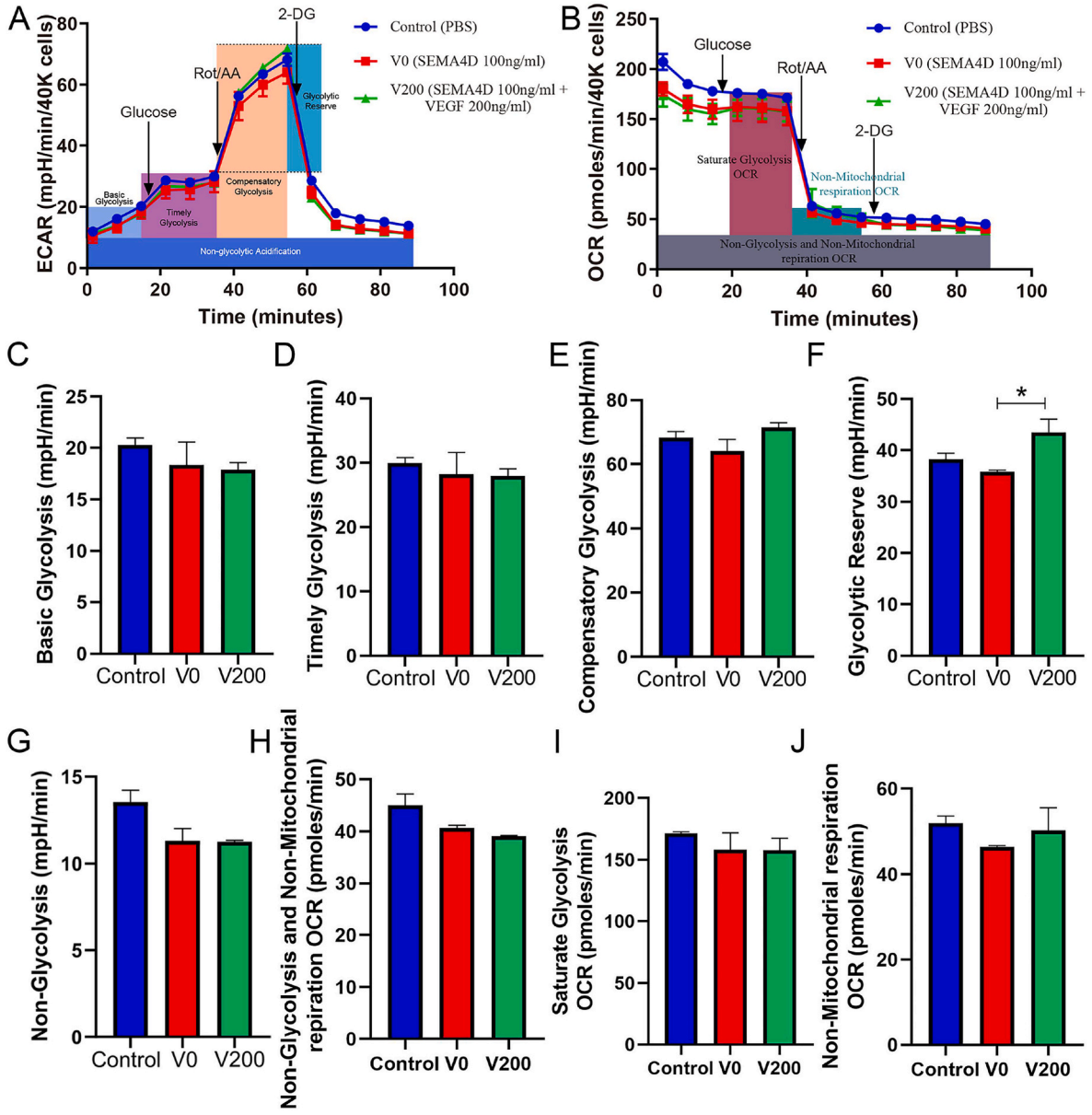

Fig. 7. Stimulated glycolysis rate. (A) Stimulated ECAR curve after different stimulus for 3h; (B) Corresponding OCR curve after 3h stimulus; Basic glycolysis (C), Timely glycolysis (D), Compensatory glycolysis (E) Glycolytic reserve (F), and Non-glycolysis (G) after 3h stimulus; non-glycolysis and non-mitochondrial respiration OCR (H), Saturate glycolysis OCR (I) and Non-mitochondrial respiration OCR (J) after 3h stimulus. Data presented as mean ± SD (n = 2) and analyzed using a one-way ANOVA, *P < 0.05.

B and H). Non-mitochondrial respiration OCR showed the oxygen needs in THP-1 stimulated by V0 or V200 are both down regulated, and V0 performance a largest decrease of oxygen demands out of mitochondrion (Fig. 7 B and J). V200 had a higher OCR than V0, and a lower OCR than control peers, suggesting V0 after stimulation has the lowest demand of oxygen, and maybe the lowest ATP production as electron transport chain and glucose input are inhibited. Overall, stimulated glycolysis had the similar trend of timely glycolysis. Stimulated glycolysis indicated that V0 and V200 stimulus can reduce macrophage glycolysis after 3h stimulation, accompanying with a largest decrease of glycolysis after V200 stimuli. Stimulated glycolysis rate assays demonstrated that THP-1 cells after V0 and V200 simuli, the glycolysis of THP-1 cells were both down regulated, representing the maximum reduction in V200 stimulated groups. The OCR reflected oxygen demand in differerent groups, V200 also represented the least oxygen demand during saturate glycolysis, demonstrating V200 stimulated THP-1 cells have the minimum activity of glycolysis. The results of stimulated glycolysis rate were consistent with the results of above timely glycolysis rate.

4. Discussion

Despite the wide employment in vascular medicine, BMS can cause mechanical injury to the blood vessel followed by local inflammatory response that further promotes the migration and proliferation of vascular SMCs and thus impedes endothelialization (Inflammation and restenosis in the stent era). Upgraded DES developed and replaced BMS to release bioactive molecules, such as anti-proliferative drugs, anti-coagulant factors and endothelialization promoted cytokines, and reduce incidents of inflammation and in-stent restenosis. Although bioresorbable stents represent less or no inflammation of the vascular wall after complete erosion [45–47], their weak mechanical properties in terms of scaffold profile, radial strength and flexibility as well as increased thrombogenicity caused by under expansion/protrusion of struts limit their application in coronary artery intervention.

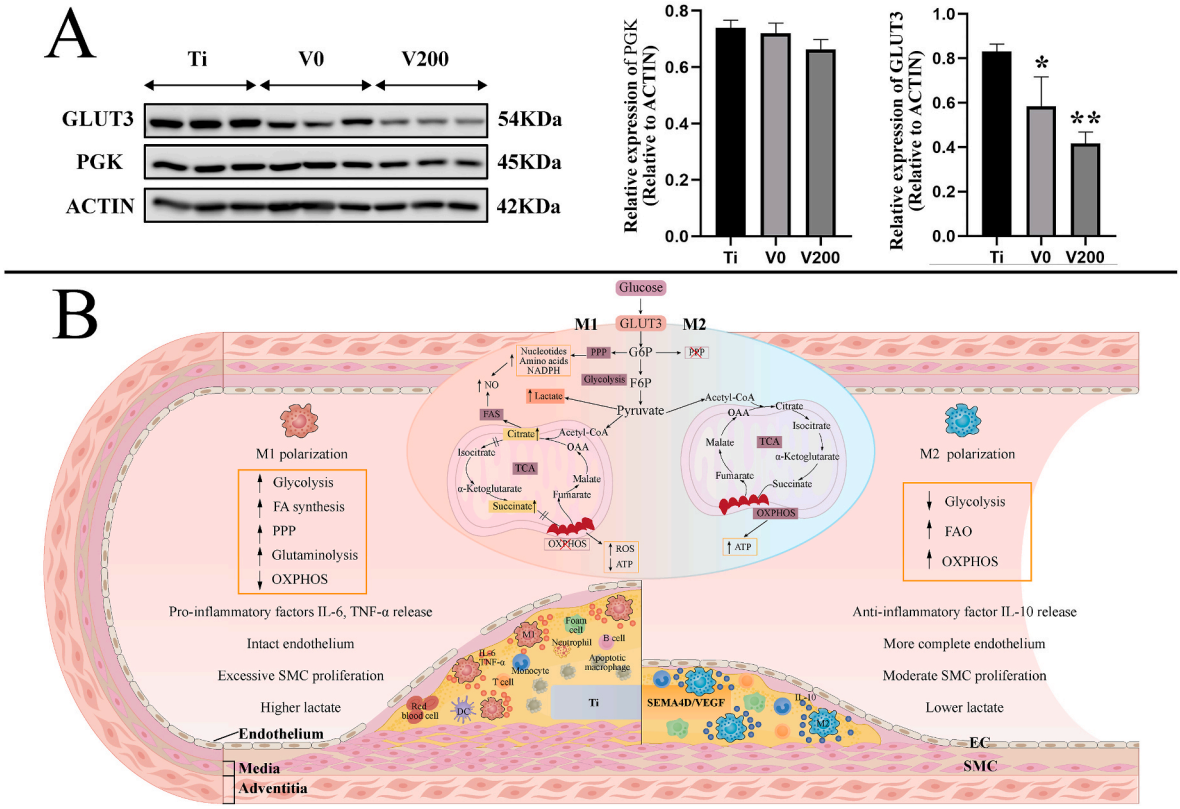

Fig. 8. The mechanism of immune cells contacting with SEMA4D/VEGF modified surfaces. (A) The expression of GLUT3 and PGK after THP-1 cultured on different modified surfaces (* denotes $P < 0.05$ compared to Ti; ** denotes $P < 0.005$ compared to Ti); (B) The role of macrophages immunometabolism of SEMA4D/VEGF modified surfaces in promoting anti-inflammatory effect and endothelialization. M1 and M2 macrophages present distinct metabolic phenotypes. Ti surfaces active more M1 macrophages, which has more catabolic metabolism, such increased glycolysis, FA synthesis, PPP, glutaminolysis, and down-regulated OXPHOX. While SEMA4D/VEGF modified surfacesstimulate more M2 macrophages, which presents more anabolic metabolism, such as increased FAO, OXPHOX, and decreased glycolysis. Rewired metabolism reprogrammed inflammatory responses of macrophages. M1 phenotype-based environment forms a necrotic center made up of apoptotic macrophages, this necrotic center would recruit other type of effect immune cells (T cell, B cell, Neutrophil, monocytes and DC) to expand inflammatory effect, thus promote the proliferation of SMC and delay the endothelialization of scaffolds. SEMA4D/VEGF modified surfaces enhance the M2 polarization and promote the repair mechanism of macrophages (release IL-10), thus exert a moderate SMC proliferation and more complete endothelium.. (GLUT3, glucose transporter 3; PGK, Phosphoglycerate kinase; FA, fatty acid; FAO, fatty acid oxidation; OXPHOS, oxidative phosphorylation; PPP, pentose phosphate pathway; ROS, reactive oxygen species; TNF, tumor necrosis factor; GLUT3, glucose transporter 3.)

Suppressing or alleviating of inflammation of implanted grafts maybe a promising strategy to solve in-stent neoatherosclerosis and restenosis.

Element detections showed element O decreased from 50 % to 45.43 % after PLL fixation, illustrating PLL successful modification onto Ti-based samples. Heparin, as an old first-line anticoagulant, has been used over a century. It is a linear, heterogeneous, highly sulfated and anionic glycosaminoglycan with relatively large molecular weight and high charge density. These specifical structural properties allow heparin easy to interact with bioactive cation proteins, leading to heparin's versatile physiologic functions, such as anticoagulant, anti-viral, anti-tumor and anti-inflammatory activities. SEMA 4D (PI = 8.5) is relative high charge of cation and can electrostatically interact with heparin under physiological environment. Successfully fixation of SEMA4D/Heparin would raise the concentration of element S (from 0 to 1.37 %) and element N (from 7.05 % to 7.67 %), both of which mainly derived from the sulfamic group of heparins, and further reduce the content of element O (from 45.43 % to 42.02 %), which mainly sourced from substrate PLL. The further combination of VEGF (PI = 8.5) would consume the active anionic group (mainly sulfamic group) from heparin, thus lowering the content of element N from 7.67 % to 5.65 %. XPS element detection demonstrated the successful modification of SEMA4D/VEGF.

In order to get good hemocompatibility of biomaterials, such as inhibit platelet adhesion and hinder thrombosis, strategies have been built to immobilize bioactive drugs or molecules onto biomimetic surfaces [48,49]. Commonly used anticoagulant, such as heparin, hirudin, resveratrol, cilostazol, triflusal, dipyridamole, and atorvastatin, have been employed to improve the hemocompatibility of biomaterial surfaces [50]. The 16-mer oligosaccharide of heparin is just long enough to form a bridge between the high-affinity pentasaccharide-binding site on antithrombin and the highly basic exosite 2 on thrombin, forming a protein-protein-oligosaccharide (antithrombin-anhydrothrombin-heparin) ternary complex, and allowing heparin active antithrombin which subsequently inhibits the activation of thrombin [51]. The blood compatibility results correlated with the heparin amounts (element S content) on the sample surfaces. Compared with V0, V200 has a lower content of surface heparin, thus represent a higher number of adhering platelets (Fig. 2 B). The fibrinogen adhesion and FGG exposure chain tests showed a similar trend as the platelet adhering (Fig. 2 D and E). P selectin reflects the activation of adhering platelets. SEMA 4D mediate platelet-platelet and platelet-endothelial cell interaction, and promote platelet activation and thus favor the formation of thrombus [26,52]. Although V0 had a high amount of heparin, its higher quantity of SEMA 4D would active platelets, and thus raise the level of P selectin (Fig. 2C). Blood hemocompatibility tests demonstrated heparin amount directly determine the adhesion of platelets and fibrinogen and the activation of fibrinogen, and SEMA 4D contributed to promote the activation of platelets.

The migration of pre-existing ECs to implanted grafts is a critical process for rapid endothelialization. The proliferation of ECs to form a

complete endothelium needs not only the chemotactic migration from the non-adjacent ECs, but also the haptotaxis migration from adjacent ECs. SEMA 4D is angiogenic in vitro and in vivo and this effect is mediated by activation of Rho, Met, and AKT signal pathways through its high-affinity receptor, Plexin B1 [30,53,54]. Besides, SEMA 4D-Plexin B1 interaction promotes the formation of focal adhesion complexes and stress fibers, as well actives the phosphorylation of the myosin light chain, consequently allowing ECs high motility [40,55,56]. Thus, samples modified by SEMA 4D (V0) had an improved proliferation function, and better haptotaxis and chemotactic migration properties (Fig. 3). VEGF pathway is well established as one of the key regulators of angiogenesis. Activation of the VEGF/VEGF-receptor axis triggers a network of signaling process that promote ECs proliferation, migration, and survival from pre-existing vasculature [57]. In addition, VEGF and SEMA4D have synergistic effects on the promotion of angiogenesis [35], and samples modified by these two factors (V200) had the best effects of ECs proliferation, as well as haptotaxis and chemotactic migration (Fig. 3).

Thrombosis and in-stent restenosis seriously impact the clinical performance of cardiovascular scaffold. In order to solve these problems, numerous strategies have been developed to fabricate hemocompatible surfaces, which could facilitate a rapid endothelialization and prevent intimal hyperplasia. Rapid endothelialization and moderate SMCs proliferation enhance the building-up of a healthy and hemocompatible endothelium. In vivo implantation study demonstrated that samples modified with SEMA4D and VEGF (V200) have the lowest level of hyperblastosis and spreading rate, and highest content of endothelium coverage and a moderate SMC layer which exert certain contractile functions. Compared to Ti control, modified samples (V0 and V200) had a better in vivo endothelialization and lower SMC proliferation (Fig. 4).

Inflammation plays an important role in development of atherosclerosis and always associated with adverse clinical outcomes in patients after percutaneous coronary interventions. The system inflammatory factor showed samples modified by SEMA4D and VEGF (V200) secrete a highest amount of anti-inflammatory factor, IL-10, and produce the lowest level of pro-inflammatory factors, IL-6 and TNF-α, demonstrating V200 promotes the formation of an anti-inflammatory environment. Compared to Ti control samples, V0 (modified by SEMA 4D) secretes a higher amount of IL-10, and the same level of IL-6 and TNF-α (Fig. 5A–C). Flow cytometry results indicate that V200 polarizes the highest amount of M2-like macrophages, and then followed by V0 and Ti control samples (Fig. 5D–G). Inflammatory factor detection and flow cytometry can confirm each other. The results of inflammatory factor and macrophage phenotype demonstrate that weak inflammatory status or anti-inflammatory tendency could promote a rapid endothelialization and prevent SMC excessive proliferation. It was reported that SEMA4D can stimulate peripheral blood monocyte polarize towards M2-like phenotype [58], supporting our research data.

Macrophages rewires their metabolic profiles in response to the changes in environmental stimuli, such as metabolic substrates or endocrine factors, and switch into anti- or pro-inflammatory phenotype. Macrophages favor glucose metabolism during disease, leading to the Warburg effect in macrophages, whereby glycolysis is favored over oxidative phosphorylation [59]. The enhanced glycolysis in macrophages leads to the release of pro-inflammatory factors, such as the secretion of IL-6, TNF-α [60]. Beyond metabolic rewiring of the macrophages and pro-inflammatory factor releasing, enhanced glycolysis signaling in these macrophages promotes epigenetic changes that also imprint M1 phenotypes in response to proinflammatory stimuli [59]. Both timely and stimulated glycolysis rate data demonstrated that V200 has the largest decrease of glycolysis rate, then followed by V0, and control groups (Figs. 6 and 7), suggesting V200 exerts the lowest tendency of pro-inflammatory status. The glycolysis rate tests further support the results of inflammatory factor detection and flow cytometry, and are proved to be an effective experimental method for detecting the inflammatory status of cardiovascular grafts. Furthermore, the expression of GLUT3 and PGK after THP-1 co-cultured with different modified surfaces for three days were tested by using western blotting (Fig. 8 A). GLUT3 is a high-affinity glucose transporter, and has a higher turnover than GLUT1 [61]. Phosphoglycerate kinase (PGK) is a rate-limiting enzyme of glycolysis. V0 samples showed lower expression of GLUT3 and PGK, and V200 showed the largest decreasing expression of GLUT3 and PGK, demonstrating after cultured on modified surfaces the glycolysis of THP1 attenuated mainly by downregulating the glucose uptake (Fig. 8 A). The molecular mechanism results further validated the timely and stimulated glycolysis rate data.

Our research elucidated the decreased glycolysis metabolism process in macrophages reshape macrophage inflammatory responses and finally resulted in an anti-inflammatory repair process around SEMA4D/VEGF modified scaffolds. The mechanism of macrophages immunometabolism of SEMA4D/VEGF modified surfaces in promoting anti-inflammatory effect and endothelialization is represented in Fig. 8. It is elucidated wired metabolic processes in macrophages reshape macrophage inflammatory responses [62]. Inflammatory macrophages need a rapid supply of energy and large consumption of bio-synthetic products as they exert to release inflammatory factors (such as IL-6 and TNF-α) fast. Anti-inflammatory macrophages need stable and continuous release of energy for long-lasting repair response [63]. Therefore, inflammatory M1 macrophages prefer an increase glucose uptake via GLUT1, enhances aerobic glycolysis and anabolism processes, such as FA synthesis, PPP as well as glutaminolysis, whereas OXPHOS of M1 macrophages via TCA is impaired [64]. Anti-inflammatory M2-like macrophages prefer the catabolism supplied continuous energy, such as FAO and OXPHOS, whereas glycolysis providing rapid energy conversion in M2-like macrophages is down regulated. M1 macrophages metabolize arginine by using inducible NO synthase to covert arginine into NO (pro-inflammatory factor) and citrulline. M2-like macrophages convert arginine to urea and ornithine [65]. NO secreted by M1 macrophages damages the mitochondrial electron-transport chain and M1 macrophages would lose the ability to polarize into M2-like macrophage, whereas M2-like phenotype could easily convert into M1 phenotype [66]. M1 phenotype-based environment forms a necrotic center made up of apoptotic macrophages, this necrotic center would recruit other type of effect immune cells (T cell, B cell, Neutrophil, monocyte and DC) to expand inflammatory effect, thus promote the proliferation of SMC and delay the endothelialization of scaffolds. SEMA4D/VEGF modified surfaces enhance the M2-like polarization and promote the repair mechanism of macrophages (release IL-10), thus exert a moderate SMCs proliferation and more complete endothelium.

5. Conclusion

In summary, we have developed a metabolism reshaped surface through electronically interaction between anticoagulant heparin and immunoregulatory SEMA4D and angiogenic VEGF. SEMA4D/VEGF co-modified coating prevents thrombogenesis, down-regulates macrophage glycolysis, promotes M2-like macrophage polarization, thus facilities the macrophage function conversion from killing to healing, and exert an endothelialization effect. In addition to the potential for addressing clinical complications (such as in-stent restenosis) of cardiovascular devices, this immunometabolism rewiring coating method also presents a promising strategy for tailoring desirable immune responses of biomedical devices by regulating immunometabolism. Immunometabolism method provide possible solution to functional material surfaces construction, characterization and clinical prediction (just as FAI, another immunometabolism index for predicating inflammation after devices clinical implantation).

Funding

This work was supported by funding from the National Natural Science Foundation of China (8200062054, 81771723), the 68th general funded project of China Postdoctoral Science Foundation (2020M683295), medical and industrial integration funded project of University of Electronic Science and Technology of China (ZYGX2021YGLH024), and the Department of Science and Technology of Sichuan Province (2022YFS0157).

Credit author statement

Yuanyuan Cui conducted the most of experiments and wrote the main manuscript text; Xiaomei Jiang , Maozhu Yang, and Yingling Yuan do the rest part of experiments and conducted data processing and analysis; Zili Zhou, Xiang Gao and Guiqing Jia provide the constructive suggestion; Lvzhou Cao, Danni Li, and Yanshuang Zhao conducted in vivo implantation experiments and taken care of the experimental animals; Xin Zhang conducted manuscript correction and polishing; Gaoping Zhao provided overall design concept and funding support.

Ethics approval and consent to participate

All experimental procedures were conducted in accordance with institutional guidelines for the care and use of laboratory animal and protocols, which were approved by the Animal Care and Use Committee of Sichuan Academy of Medical Sciences & Sichuan Provincial People's Hospital, Chengdu, China.

Consent for publication

We give our consent for the manuscript to the published in Materials Today Bio.

Author dummy statement

The data that support the findings of this study are available from the corresponding author upon reasonable request.

Declaration of competing interest

The authors declared no potential conflicts of interest with respect to the research, author-ship, and/or publication of this article.

Data availability

Data will be made available on request.

Acknowledgements

Not applicable.

References

[1] R. Hajar, Framingham contribution to cardiovascular disease, Heart Views : Offl. J. Gulf Heart Assoc. 17 (2016) 78–81, https://doi.org/10.4103/1995-705x.185130.
[2] J. Zhao, Y. Feng, Surface engineering of cardiovascular devices for improved hemocompatibility and rapid endothelialization, Adv. Healthcare Mater. 9 (2020), e2000920, https://doi.org/10.1002/adhm.202000920.
[3] S. Jana, Endothelialization of cardiovascular devices, Acta Biomater. 99 (2019) 53–71, https://doi.org/10.1016/j.actbio.2019.08.042.
[4] A. Scafa Udriște, A.G. Niculescu, A.M. Grumezescu, E. Bădilă, Cardiovascular stents: a review of past, current, and emerging devices, Materials 14 (2021), https://doi.org/10.3390/ma14102498.
[5] Y. Yang, et al., Endothelium-Mimicking multifunctional coating modified cardiovascular stents via a stepwise metal-catechol-(amine) surface engineering strategy, Research (2020), 9203906, https://doi.org/10.34133/2020/9203906 (2020).
[6] P.P. Karjalainen, W. Nammas, Titanium-nitride-oxide-coated coronary stents: insights from the available evidence, Ann. Med. 49 (2017) 299–309, https://doi.org/10.1080/07853890.2016.1244353.
[7] D. Ochijewicz, M. Tomaniak, G. Opolski, J. Kochman, Inflammation as a determinant of healing response after coronary stent implantation, Int. J. Cardiovasc. Imag. 37 (2021) 791–801, https://doi.org/10.1007/s10554-020-02073-3.
[8] K. Miwa, et al., Comparison of sirolimus-eluting, paclitaxel-eluting, and bare-metal stents in a patient with angina pectoris: histopathological autopsy findings of the third month, Cardiovas. Interv. Therap. 29 (2014) 334–338, https://doi.org/10.1007/s12928-013-0233-5.
[9] T. Barrett, J. Macrophages in atherosclerosis regression, Arterioscler. Thromb. Vasc. Biol. 40 (2020) 20–33, https://doi.org/10.1161/atvbaha.119.312802.
[10] D.M. Mosser, J.P. Edwards, Exploring the full spectrum of macrophage activation, Nat. Rev. Immunol. 8 (2008) 958–969, https://doi.org/10.1038/nri2448.
[11] S.C. Huang, et al., Cell-intrinsic lysosomal lipolysis is essential for alternative activation of macrophages, Nat. Immunol. 15 (2014) 846–855, https://doi.org/10.1038/ni.2956.
[12] C. Cui, M. Wen, F. Zhou, Y. Zhao, X. Yuan, Target regulation of both VECs and VSMCs by dual-loading miRNA-126 and miRNA-145 in the bilayered electrospun membrane for small-diameter vascular regeneration, J. Biomed. Mater. Res., Part A 107 (2019) 371–382, https://doi.org/10.1002/jbm.a.36548.
[13] J. Wang, et al., miR-22 eluting cardiovascular stent based on a self-healable spongy coating inhibits in-stent restenosis, Bioact. Mater. 6 (2021) 4686–4696, https://doi.org/10.1016/j.bioactmat.2021.04.037.
[14] M. Wen, et al., Local delivery of dual MicroRNAs in trilayered electrospun grafts for vascular regeneration, ACS Appl. Mater. Interfaces 12 (2020) 6863–6875, https://doi.org/10.1021/acsami.9b19452.
[15] Y. Wei, et al., MSC-derived sEVs enhance patency and inhibit calcification of synthetic vascular grafts by immunomodulation in a rat model of hyperlipidemia, Biomaterials 204 (2019) 13–24, https://doi.org/10.1016/j.biomaterials.2019.01.049.
[16] G. Caputa, A. Castoldi, E.J. Pearce, Metabolic adaptations of tissue-resident immune cells, Nat. Immunol. 20 (2019) 793–801, https://doi.org/10.1038/s41590-019-0407-0.
[17] E.K. Oikonomou, et al., Non-invasive detection of coronary inflammation using computed tomography and prediction of residual cardiovascular risk (the CRISP CT study): a post-hoc analysis of prospective outcome data, Lancet (London, England) 392 (2018) 929–939, https://doi.org/10.1016/s0140-6736(18)31114-0.
[18] A.S. Antonopoulos, A. Angelopoulos, K. Tsioufis, C. Antoniades, D. Tousoulis, Cardiovascular risk stratification by coronary computed tomography angiography imaging: current state-of-the-art, Eur. J. Prevent. Cardiol. 29 (2022) 608–624, https://doi.org/10.1093/eurjpc/zwab067.
[19] B. Qin, et al., The predictive value of the perivascular adipose tissue CT fat attenuation index for coronary in-stent restenosis, Front. Cardiovas. Med. 9 (2022), 822308, https://doi.org/10.3389/fcvm.2022.822308.
[20] K.T. Maleki, M. Cornillet, N.K. Björkström, Soluble SEMA4D/CD100: a novel immunoregulator in infectious and inflammatory diseases, Clinical immunology (Orlando, Fla 163 (2016) 52–59, https://doi.org/10.1016/j.clim.2015.12.012.
[21] W. Shi, et al., The class IV semaphorin CD100 plays nonredundant roles in the immune system: defective B and T cell activation in CD100-deficient mice, Immunity 13 (2000) 633–642, https://doi.org/10.1016/s1074-7613(00)00063-7.
[22] M. Li, et al., Endogenous CD100 promotes glomerular injury and macrophage recruitment in experimental crescentic glomerulonephritis, Immunology 128 (2009) 114–122, https://doi.org/10.1111/j.1365-2567.2009.03098.x.
[23] X. Jiang, N.K. Björkström, E. Melum, Intact cd100-CD72 interaction necessary for TCR-induced T cell proliferation, Front. Immunol. 8 (2017) 765, https://doi.org/10.3389/fimmu.2017.00765.
[24] B. Liu, et al., CD8low CD100- T cells identify a novel CD8 T cell subset associated with viral control during human hantaan virus infection, J. Virol. 89 (2015) 11834–11844, https://doi.org/10.1128/jvi.01610-15.
[25] S. Mizrahi, G. Markel, A. Porgador, Y. Bushkin, O. Mandelboim, CD100 on NK cells enhance IFNgamma secretion and killing of target cells expressing CD72, PLoS One 2 (2007) e818, https://doi.org/10.1371/journal.pone.0000818.
[26] L. Zhu, et al., Regulated surface expression and shedding support a dual role for semaphorin 4D in platelet responses to vascular injury, Proc. Natl. Acad. Sci. U. S. A. 104 (2007) 1621–1626, https://doi.org/10.1073/pnas.0606344104.
[27] M.C. Luque, et al., Phage display identification of CD100 in human atherosclerotic plaque macrophages and foam cells, PLoS One 8 (2013), e75772, https://doi.org/10.1371/journal.pone.0075772.
[28] C. Bougeret, et al., Increased surface expression of a newly identified 150-kDa dimer early after human T lymphocyte activation, J. Immunol. 148 (1992) 318–323. Baltimore, Md. : 1950.
[29] H. Kikutani, A. Kumanogoh, Semaphorins in interactions between T cells and antigen-presenting cells, Nat. Rev. Immunol. 3 (2003) 159–167, https://doi.org/10.1038/nri1003.
[30] P. Conrotto, et al., Sema4D induces angiogenesis through Met recruitment by Plexin B1, Blood 105 (2005) 4321–4329, https://doi.org/10.1182/blood-2004-07-2885.
[31] Y. Cui, et al., Situ endothelialization promoted by SEMA4D and CXCL12 for titanium-based biomaterials, Semin. Thromb. Hemost. 44 (2018) 70–80, https://doi.org/10.1055/s-0037-1605569.
[32] Y. Cui, et al., SEMA4D-heparin complexes immobilized on titanium surfaces have anticoagulant, cell-migration-promoting, and immunoregulatory effects, ACS Biomater. Sci. Eng. 4 (2018) 1598–1608, https://doi.org/10.1021/acsbiomaterials.8b00098.

[33] Y. Cui, et al., Real-time QCM-D monitoring of endothelial cells and macrophages adhering and spreading to SEMA4D/heparin surfaces, Colloids Surf. B Biointerfaces 171 (2018) 522–529, https://doi.org/10.1016/j.colsurfb.2018.07.062.
[34] N. Ferrara, Vascular endothelial growth factor: basic science and clinical progress, Endocr. Rev. 25 (2004) 581–611, https://doi.org/10.1210/er.2003-0027.
[35] Y. Chen, L. Zhang, W.X. Liu, K. Wang, VEGF and SEMA4D have synergistic effects on the promotion of angiogenesis in epithelial ovarian cancer, Cell. Mol. Biol. Lett. 23 (2018) 2, https://doi.org/10.1186/s11658-017-0058-9.
[36] S.A. Smith, R.J. Travers, J.H. Morrissey, How it all starts: initiation of the clotting cascade, Crit. Rev. Biochem. Mol. Biol. 50 (2015) 326–336, https://doi.org/10.3109/10409238.2015.1050550.
[37] H.H. Versteeg, J.W. Heemskerk, M. Levi, P.H. Reitsma, New fundamentals in hemostasis, Physiol. Rev. 93 (2013) 327–358, https://doi.org/10.1152/physrev.00016.2011.
[38] D.P. Mikhailidis, M.A. Barradas, A. Maris, J.Y. Jeremy, P. Dandona, Fibrinogen mediated activation of platelet aggregation and thromboxane A2 release: pathological implications in vascular disease, J. Clin. Pathol. 38 (1985) 1166–1171, https://doi.org/10.1136/jcp.38.10.1166.
[39] S. Karaman, V.M. Leppänen, K. Alitalo, Vascular Endothelial Growth Factor Signaling in Development and Disease, Development, Cambridge, England, 2018, https://doi.org/10.1242/dev.151019, 145.
[40] J.R. Basile, A. Barac, T. Zhu, K.L. Guan, J.S. Gutkind, Class IV semaphorins promote angiogenesis by stimulating Rho-initiated pathways through plexin-B, Cancer Res. 64 (2004) 5212–5224, https://doi.org/10.1158/0008-5472.Can-04-0126.
[41] L. Liu, et al., SEMA4D/PlexinB1 promotes AML progression via activation of PI3K/Akt signaling, J. Transl. Med. 20 (2022) 304, https://doi.org/10.1186/s12967-022-03500-w.
[42] S. Déglise, C. Bechelli, F. Allagnat, Vascular smooth muscle cells in intimal hyperplasia, an update, Front. Physiol. 13 (2022), 1081881, https://doi.org/10.3389/fphys.2022.1081881.
[43] S. Eligini, E. Gianazza, A. Mallia, S. Ghilardi, C. Banfi, Macrophage phenotyping in atherosclerosis by proteomics, Int. J. Mol. Sci. 24 (2023), https://doi.org/10.3390/ijms24032613.
[44] A.J. Mouton, X. Li, M.E. Hall, J.E. Hall, Obesity, hypertension, and cardiac dysfunction: novel roles of immunometabolism in macrophage activation and inflammation, Circ. Res. 126 (2020) 789–806, https://doi.org/10.1161/circresaha.119.312321.
[45] A. Sumida, et al., A comparison of drug eluting stent biocompatibility between third generation NOBORI biolimus A9-eluting stent and second generation XIENCE V everolimus-eluting stent in a porcine coronary artery model, Cardiovasc. Revasculariz. Med. : Mol. Interv. 16 (2015) 351–357, https://doi.org/10.1016/j.carrev.2015.06.009.
[46] M. Kozel, V. Kočka, L. Lisa, T. Buděšínský, P. Toušek, Immune-inflammatory response after bioresorbable vascular scaffold implantation in patients with acute myocardial infarction with ST elevation in a long-term perspective, Heart Ves. 34 (2019) 557–563, https://doi.org/10.1007/s00380-018-1281-7.
[47] R. Rampat, et al., Association between inflammatory biomarkers and neointimal response following elective implantation of the ABSORB bioresorbable vascular scaffold, Coron. Artery Dis. 30 (2019) 183–187, https://doi.org/10.1097/mca.0000000000000699.
[48] Q. Zhang, et al., Heparinization and hybridization of electrospun tubular graft for improved endothelialization and anticoagulation, Mater. Sci. Eng., C 122 (2021), 111861, https://doi.org/10.1016/j.msec.2020.111861.
[49] B. Zhang, et al., Epigallocatechin gallate mediated sandwich-like coating for mimicking endothelium with sustained therapeutic nitric oxide generation and heparin release, Biomaterials 269 (2021), 120418, https://doi.org/10.1016/j.biomaterials.2020.120418.
[50] L.A. Feng, J. Shi, J.Y. Guo, S.F. Wang, Recent strategies for improving hemocompatibility and endothelialization of cardiovascular devices and inhibition of intimal hyperplasia, J. Mater. Chem. B 10 (2022) 3781–3792, https://doi.org/10.1039/d2tb00478j.
[51] A. Dementiev, M. Petitou, J.M. Herbert, P.G. Gettins, The ternary complex of antithrombin-anhydrothrombin-heparin reveals the basis of inhibitor specificity, Nat. Struct. Mol. Biol. 11 (2004) 863–867, https://doi.org/10.1038/nsmb810.
[52] L. Zhu, et al., Disruption of SEMA4D ameliorates platelet hypersensitivity in dyslipidemia and confers protection against the development of atherosclerosis, Arterioscler. Thromb. Vasc. Biol. 29 (2009) 1039–1045, https://doi.org/10.1161/atvbaha.109.185405.
[53] A. Sakurai, C.L. Doçi, J.S. Gutkind, Semaphorin signaling in angiogenesis, lymphangiogenesis and cancer, Cell Res. 22 (2012) 23–32, https://doi.org/10.1038/cr.2011.198.
[54] G. Neufeld, O. Kessler, The semaphorins: versatile regulators of tumour progression and tumour angiogenesis, Nat. Rev. Cancer 8 (2008) 632–645, https://doi.org/10.1038/nrc2404.
[55] J.R. Basile, J. Gavard, J.S. Gutkind, Plexin-B1 utilizes RhoA and Rho kinase to promote the integrin-dependent activation of Akt and ERK and endothelial cell motility, J. Biol. Chem. 282 (2007) 34888–34895, https://doi.org/10.1074/jbc.M705467200.
[56] J.R. Basile, T. Afkhami, J.S. Gutkind, Semaphorin 4D/plexin-B1 induces endothelial cell migration through the activation of PYK2, Src, and the phosphatidylinositol 3-kinase-Akt pathway, Mol. Cell Biol. 25 (2005) 6889–6898, https://doi.org/10.1128/mcb.25.16.6889-6898.2005.
[57] D.J. Hicklin, L.M. Ellis, Role of the vascular endothelial growth factor pathway in tumor growth and angiogenesis, J. Clin. Oncol. : Offl. J. Am. Soc. Clin. Oncol. 23 (2005) 1011–1027, https://doi.org/10.1200/jco.2005.06.081.
[58] Y. Chen, L. Zhang, R. Lv, W.Q. Zhang, Overexpression of Semaphorin4D indicates poor prognosis and prompts monocyte differentiation toward M2 macrophages in epithelial ovarian cancer, Asian Pac. J. Cancer Prev. APJCP : Asian Pac. J. Cancer Prev. APJCP 14 (2013) 5883–5890, https://doi.org/10.7314/apjcp.2013.14.10.5883.
[59] A. Rasheed, K.J. Rayner, Macrophage responses to environmental stimuli during homeostasis and disease, Endocr. Rev. 42 (2021) 407–435, https://doi.org/10.1210/endrev/bnab004.
[60] R. Watanabe, et al., Glucose metabolism controls disease-specific signatures of macrophage effector functions, JCI insight 3 (2018), https://doi.org/10.1172/jci.insight.123047.
[61] A. Suades, et al., Establishing mammalian GLUT kinetics and lipid composition influences in a reconstituted-liposome system, Nat. Commun. 14 (2023) 4070, https://doi.org/10.1038/s41467-023-39711-y.
[62] G.J. Koelwyn, E.M. Corr, E. Erbay, K.J. Moore, Regulation of macrophage immunometabolism in atherosclerosis, Nat. Immunol. 19 (2018) 526–537, https://doi.org/10.1038/s41590-018-0113-3.
[63] D.F.J. Ketelhuth, et al., Immunometabolism and atherosclerosis: perspectives and clinical significance: a position paper from the working group on atherosclerosis and vascular biology of the European society of cardiology, Cardiovasc. Res. 115 (2019) 1385–1392, https://doi.org/10.1093/cvr/cvz166.
[64] A.K. Jha, et al., Network integration of parallel metabolic and transcriptional data reveals metabolic modules that regulate macrophage polarization, Immunity 42 (2015) 419–430, https://doi.org/10.1016/j.immuni.2015.02.005.
[65] K. Ley, M1 means kill; M2 means heal, J. Immunol. 199 (2017) 2191–2193, https://doi.org/10.4049/jimmunol.1701135. Baltimore, Md. 1950.
[66] J. Van den Bossche, et al., Mitochondrial dysfunction prevents repolarization of inflammatory macrophages, Cell Rep. 17 (2016) 684–696, https://doi.org/10.1016/j.celrep.2016.09.008.